Halothane Solvation in Water and Organic Solvents from Molecular Simulations with New Polarizable Potential Function

Julia O. Subbotina,[†,§] Jonathan Johannes,[‡,§] Bogdan Lev,[†] and Sergei Yu Noskov*[,†]

Institute for BioComplexity and Informatics and Department for Biological Sciences, University of Calgary, 2500 University Drive, Calgary, AB, Canada T2N 1N4, and Department of Physics and Astronomy, 6224 Agricultural Road, University of British Columbia, Vancouver, BC, V6T 1Z1 Canada

Received: August 28, 2009; Revised Manuscript Received: March 16, 2010

The partitioning of a substrate from one phase into another is a complex process with widespread applications: from chemical technology to the pharmaceutical industry. One particularly well-known and well-studied example is 2-bromo-2-chloro-1,1,1-trifluoroethane (*halothane*) trafficking through the lipid bilayer. Halothane is a model volatile anesthetic known to impact functions of model lipid bilayers, altering the structure and thickness upon its partitioning from the bulk phase. A number of theoretical and experimental investigations suggest the importance of electronic polarizability, determining a preference for halothane to partition in the interfacial systems as in lipid bilayers or binary solvents. The recently published protocol for the development of polarizable force fields based on the classical Drude model has provided fresh impetus to efforts directed at understanding the molecular principles governing complex thermodynamics of the hydrophobic hydration. Here, molecular simulations were combined with free energy simulations to study solvation of halothane in polarizable water and methanol. The absolute free energy of halothane solvation in different solvents (water, methanol, and *n*-hexane) has been evaluated for additive and polarizable models. It was found that both additive and polarizable models provide an adequate description of the halothane solvation in high-dielectric (polar) solvents such as water, but explicit accounting for electronic polarization is imperative for a correct description of the solvation thermodynamics in nonpolar systems. To study halothane dynamics in binary mixtures, all-atom molecular dynamics (MD) simulations for halothane−methanol mixtures in a wide range of concentrations were performed alongside an analysis of structural organization, dynamics, and thermodynamic properties to dissect the molecular determinants of the halothane solvation in polar and amphiphilic liquids such as methanol. Additionally, a theoretical test of the hypothesis on the weak hydrogen bonding of halothane and methanol in the condensed phase is provided, which was presented on the basis of spectroscopic analysis of the C−H vibrations in different gas-phase complexes. The simulations performed in the condensed phase suggest that hydrophobic interactions between halothane and methanol play a dominant role in preferential solvation.

1. Introduction

Halothane is an inhalational general anesthetic listed as a core medicine by the World Health Organization.[1] Despite an impressive body of literature, the exact molecular mechanism of action for general anesthetics remains a hotly debated topic.[1−3] Two main explanations have been proposed: one is based on the well-established Overton−Meyer principles relating oil (fat) solubility of general anesthetics and their anesthetic potency,[4] where partitioning of the drug into the membrane alters key physicochemical properties of the lipid bilayer, thereby inhibiting membrane protein function.[3,5] With the development of instrumental techniques a second mechanism was proposed emphasizing the importance of protein−drug interaction for the general anesthesia.[6] In particular, a number of ligand-gated ion channels[6−8] have been identified to be important targets for halothane and other general anesthetics. Realistically, it is likely that both explanations are valid and the actual system is more complex than simply a single model.[9] If this is the case, one has to ascertain detailed knowledge of the molecular interactions of halothane, model membranes, and membrane proteins to render a comprehensive mechanism of action for volatile anesthetics.[10]

Approaches based on atomistic simulations, such as molecular dynamics or Monte Carlo, may provide, arguably, the most detailed description of the interactions between volatile anesthetics and model membranes/peptides at the atomistic level. Expectedly, several theoretical papers have appeared on mechanisms of anesthetics partitioning into lipid bilayers, binding to channels and receptors, and the theoretical development of the halothane force fields,[8,10−13] including the most recent effort from the Klein group to parametrize isoflurane.[14] One of the most detailed reports on the determination of potential parameters for halothane was published by the Tang group.[11,15] The developed parameters achieved a correct description of neat halothane, thus supplying the scientific community with a reliable additive force field. Similar to conditions for other additive potential models, the charge distribution between atomic sites in halothane was fixed to reproduce relevant thermodynamic properties of neat and aqueous halothane, thus providing an implicit account for electronic polarizability of the molecule. This model was successfully implemented to study halothane

* Author for correspondence. Phone: 403-220-2425. Fax: 403-210-8655. E-mail: snoskov@ucalgary.ca.
† University of Calgary.
‡ University of British Columbia.
§ Both authors contributed equally to this manuscript.

10.1021/jp908339j
Published on Web 04/22/2010

TABLE 1: Potential Model for Polarizable and Additive Halothane Models

	additive 1		ab initio		additive 2			drude			
parameter	q (e)	QM (e)	NBO[b] (e)	QM[c] (e)	q (e)	ε (kcal/mol)	$R_{min}/2$ (Å)	q (e)	ε (kcal/mol)	$R_{min}/2$ (Å)	α (Å^3)
C1	0.490	1.776	1.123	1.593	0.130	−0.078	2.040	0.354	−0.078	2.090	−1.411
F	−0.170	−0.617 −0.620 −0.623	−0.366	−0.399	−0.047	−0.098[a]	1.635[a]	−0.118	−0.082	1.675	−0.745
C2	0.010	0.076	−0.414	−0.653	−0.099	−0.078	2.040	−0.044	−0.078	2.090	−1.980
H21	0.100	0.193	0.276	0.000	0.102	−0.046	0.224	0.130	−0.019	1.210	−
Cl2	−0.060	0.014	0.022	−0.004	0.088	−0.254[a]	1.981[a]	−0.025	−0.203	1.980	−2.125
Br2	−0.030	0.028	0.090	0.280	−0.080	−0.314[a]	2.099[a]	−0.061	−0.321	2.110	−2.952

[a] Additive 1 is model developed by Liu et al.,[15] Additive 2 is a additive model developed in this work. Drude abbreviates for the polarizable model. [b] Charges extracted from the natural bond orbitals analysis[70] performed at the B3LYP/aug-cc-pvdz level of theory. [c] Mulliken atomic charges determined at the same level of theory.

binding to potassium channels[8] and the nicotinic acetylcholine receptor (nAChR).[16] However, several experimental studies addressing halothane solvation in methanol, benzene, phenol, and other common organic solvents suggest that halo compounds may be capable of forming weak hydrogen bonds[17,18] due to their high molecular polarizability. An explicit account for electronic polarizability[19,20] may be required for studies of individual halothane interactions with proton acceptors. The presence of a permanent or induced dipole moment is thought to be important for the anesthetic ability of the molecule.[21] Furthermore, the explicit accounting for electronic polarization of the hydrocarbon tails and polar heads in lipids was shown to have a major impact on evaluations of complex electrostatic effects that led to the formation of membrane potentials experienced by the solute.[22−25]

The work on the polarizable force field for the lipid simulations is ongoing,[26,27] but it is possible to start analyzing model mixtures of halothane with relevant organic solvents, thereby quantifying the role of electronic polarization in solvation thermodynamics. In this report, polarizable and additive halothane models that are compatible with the CHARMM Drude force field have been developed. To further validate our model and to provide additional insight on how explicit polarization affects conclusions on the halothane dynamics in different solvents, we report on the halothane solvation and solubility in polarizable water, *n*-hexane, and binary mixtures with methanol.

2. Methodological Details

Development of Potential Models. To address the apparent need in the polarizable force fields for common solvents and solutes, a robust protocol to parametrize halothane based on the classical Drude model[28−32] was effected. The cornerstones of the parametrization are ab initio computations combined with MD simulations, which correctly target most of the reported thermodynamic data. Most of the potential functions are being developed with the free energy of hydration as a target property. An auxiliary Drude particle is tethered to every heavy atom site (C, Cl, Br, F) in accord with previously developed protocol. All intramolecular parameters for both polarizable and additive models are summarized in Table S1 of the Supporting Information. The molecular electrostatic potential (ESP) maps were obtained for geometries optimized at the MP2(fc)/6-31G(d) level of theory, using the B3LYP hybrid functional[33,34] and the correlation-consistent double-ζ Dunning aug-cc-pVDZ basis set.[35] A torsional scan along the C−C axis and spectral analysis were performed at the same level of theory and basis set to determine the minimal energy conformation of the halothane molecule. Spectral bond, angle, and dihedral vibrations and torsions were obtained using a protocol developed by Pulay et al.[36] Torsion profiles for principal dihedrals were obtained by a rotational scan at the MP2/cc-pVDZ level (Figure S1 in the Supporting Information). All QM calculations were performed with the Gaussian 03 suite of programs.[37] It should be noted that to enable efficient comparison between polarizable and additive models, we have parametrized them both using similar protocols. The determination of the electrostatic parameters for the model, i.e., the atomic charges and polarizabilities, is a critical stage in the model development for the Drude polarizable force field.[38] Initial values of the partial atomic charges and polarizabilities used in fitting were taken from the NBO-derived charges and from atomic polarizability (α) values reported previously.[39] Partial atomic charges and atomic polarizabilities were adjusted following restrained fitting to QM perturbed ESP maps.[38] The subsequent fitting was performed with parabolic restraints to the initial values of both the charges and the polarizabilities with the weighting factor of 10^{-6} e^{-2}. A flat well potential with a half-width of 0.1 e was introduced for atomic polarizabilities. All bond, angle, and dihedral coefficients were determined by fitting these intramolecular parameters to the energy profile and spectral data gained from ab initio calculations. The torsional scans performed on halothane were calculated through a 180° rotation, incrementing the Br2−C2−C1−F dihedral angle by 10° from 0°. The result is as expected, and all models are in agreement: the staggered forms at 60° and 180° are the minimal energy conformations, and the eclipsed forms at 0° and 120° are the less favorable high-energy conformations. The remaining 180°, completing the 360° rotation would simply be a repetition of what is seen in Figure S1 (Supporting Information). The energetic profile has a sinusoidal form with a period of 120° due to the internal symmetry of the halothane structure. The overall higher energies apparent in the polarizable model can be attributed to the presence of the Drude particles adding to the steric hindrances of the eclipsed forms.

Lennard-Jones parameters were then optimized in an iterative manner.[40] Initial guesses for the Lennard-Jones parameters for the additive model were extracted from the model developed before.[41] At the next step Lennard-Jones parameters were adjusted to yield condensed-phase properties, such as enthalpy of vaporization, self-diffusion coefficient, and dielectric constant via MD simulations. The resulting parameters for the additive and polarizable halothane models are summarized in Table 1, along with reference values from experimental data and ab initio calculations.

Molecular Dynamics Simulation Protocol. To compute thermodynamic and dynamic properties of neat halothane and its mixtures with methanol, *n*-hexane, and water, a total of 250

solute/solvent molecules were simulated with molecular dynamics in a cubic box with periodic boundary conditions in the *NPT* ensemble. For all mixtures, the concentrations are reported for the mole fractions of halothane (X_1). The potential parameters for all solvents were developed previously.[38,42,43] Electrostatic interactions were computed with particle-mesh Ewald summation, with $\kappa = 0.34$ for the charge screening and a 0.8 Å grid spacing. The real-space interactions (both Lennard-Jones and electrostatic) were cut off at 18 Å, and long-range contributions were corrected with an average density-dependent term (Lennard-Jones long-range correction).[29] The temperature of the system was controlled with a two-thermostat algorithm, where atoms were kept at room temperature (298.15 K), whereas auxiliary Drude particles were kept at a low temperature (1 K) to ensure the self-consistent induction regime. A 1 fs time step with a multistep integration scheme for the thermostat variables was implemented. Two aqueous solutions were simulated: the TIP3 water model was used in conjunction with the additive halothane, and the SWM4-NDP polarizable water model[29] was used with the polarizable halothane simulations of aqueous solutions with a mass of 0.4 au on the auxiliary Drude particles and a force constant $k = 1000$ (kcal/mol)/Å^2 for the atom−Drude coupling. A similar approach was taken for halothane−methanol solutions. The additive model of methanol was used with the additive halothane for estimations on the free energy of solvation, and the polarizable methanol model was used for studies of the polarizable halothane solvation in methanol.[42] Self-diffusion, dielectric constants, and heats of vaporization for polarizable and additive models have been evaluated using standard protocols, and the interested reader can find details elsewhere.[30,32,44]

Evaluation of the Free Energy of Solvation in Water and Organic Solvents. The free energy of halothane solvation in water and methanol was evaluated using the standard free energy perturbation (FEP)/MD protocols, similar to those implemented in previous studies of absolute solvation free energies.[45−47] To further improve the convergence of the nonelectrostatic contributions to the free energy of solvation, the Weeks−Chandler−Anderson (WCA) decomposition of the Lennard-Jones interaction was used.[48−50] According to the WCA theory, the Lennard-Jones potential can be arbitrarily separated into repulsive and dispersive-free energies, referred to in this paper as ΔG_{rep} and ΔG_{disp}, respectively. The nonlinear-coupling parameter ξ was used to control the repulsive portion in the FEP simulations, and the linear coupling parameter γ was used for the evaluation of the dispersive contribution. In addition, the linear-coupling parameter l was used for all FEP/MD simulations to control electrostatic contributions to the free energy. The repulsive interaction was turned on first ($\xi = 0$, 0.1, 0.2,0.3, 0.4, 0.5, 0.6, 0.7, 0.8, 0.9, and 1.0) with both electrostatic and dispersive interactions being turned off. Next, the dispersive interactions between the solute and environment were turned on in the presence of the full repulsion, with $\gamma = 0.0$, 0.25, 0.5, 0.75, and 1.0. Finally, the electrostatic interactions were gradually turned on, with $\lambda = 0.0$, 0.1, 0.2, 0.3, 0.4, 0.5, 0.6, 0.7, 0.8, 0.9, and 1.0 in the presence of both repulsion and dispersion in the system to evaluate electrostatic free energy ΔG_{elec}. For each window, 250 ps of Langevin dynamics (LD) was performed first to equilibrate the system and then 2500 ps of NPT simulation to obtain statistics for the WHAM postanalysis.[51,52]

Cluster Analysis. To analyze the hydrogen-bonded clusters present in the binary halothane−methanol solutions, we have monitored the statistics of close contacts between H-bond donors and acceptors. The previously developed algorithm for cluster size distributions has been used. The statistics have been collected every 1 ps over the course of the last 8 ns of trajectory. Two types of H-bonded clusters have been considered: homogeneous, formed by methanol molecules only, and heterogeneous, with the possibility of the hydrogen bonding between oxygen from the hydroxyl group of methanol and the only hydrogen atom of halothane. For the present analysis, two molecules are considered to be connected if the H---O and O---O distances are less than 2.5 and 3.5 Å, respectively, and their O−H---O or C−H---O angle is larger than 140°. Some research reports suggest the use of carbon−carbon distances for clustering of methanol as well.[53] Our major focus was, however, on the hydrogen bonding between halothane and methanol.

3. Results and Discussion

Dipole Moment and Dielectric Constants from Simulations with Polarizable and Additive Models. The first step in validating the potential model is to examine reproducibility of the geometries and dipole moments from previous studies. Table 1 summarizes the geometries for the present polarizable model along with available potential models. It should be noted that results for the equilibrium geometries are similar to those from previous studies using additive potential functions and high-level quantum chemistry computations.[8,11,41] The resulting gas-phase dipole moment differs modestly between additive and polarizable potential functions by about 0.2 D, which is consistent with the development of polarizable models for other compounds.[54] The reported experimental values are around 1.4 D for infinitely diluted halothane in chloroform and likely contain contributions from induced dipoles due to the solvent field,[55] whereas the value of 1.24 D was obtained from high-level ab initio computations.[20] The change in molecular dipole moment of halothane transferring from the gas phase to the bulk phase is a good indicator of the condensed-phase polarization effect and indicates the importance of accounting for the induced polarization. The theoretical results from atomistic simulations with flexible potential model built from Car−Parrinello energy minimization indicate the full dipole moment of the neat halothane to be ∼2−2.2 D and similarly adjusted dipole moments were used in previous atomistic and coarse-grained MD simulations.[56] The average dipole moment in the bulk phase for the polarizable model developed in this paper is ∼1.9−2.1 D. An induced dipole moment of the halothane molecule in the bulk phase is around 0.7−0.8 D. The importance of having a dipole moment of about ∼2 D[7,12,13] for halothane was emphasized for proper partitioning close to the carbonyl groups of the lipids in the membrane.[56] In comparison, an induced dipole of halothane in polarizable water is ∼0.3 D (1.4 D), whereas an induced dipole in methanol is ∼0.5 D (1.7 D). The values in parentheses correspond to the full dipole of the halothane molecule. The induced dipole of halothane depends strongly on the environment (low dielectric neat halothane with $\varepsilon = 4$, amphipathic solvent such as methanol with $\varepsilon = 32$ and polar water with $\varepsilon = 80$). The explicit treatment for the electronic polarizability has had a major impact for simulating dielectric constants for the neat liquid. The dielectric constant for polarizable model was 4.12 against the experimental value ∼4.0, while the additive model averaged around a value of 2.4.

Liquid Halothane: Thermodynamics, Diffusion Properties, and Structure. The simulated and experimental results on enthalpy of evaporation, density of the neat liquid at room temperature, self-diffusion coefficients, and dielectric constants are presented in Table 2 for various potential models. The performances of the additive and polarizable models reproducing thermodynamical data and density are comparable and agree

TABLE 2: Properties of Liquid Halothane at $T = 298.15$ K

model	H_{evap}, kcal/mol[a]	ρ, g/cm^3	D, 10^5 cm^2 s^{-1}	ε	ΔG_{hydr}, kcal/mol	ΔG_{MeOH}, kcal/mol	μ (D)	D_{H_2O}, 10^5 cm^2 s^{-1} [b]	D_{MeOH}, 10^5 cm^2 s^{-1} [b]
exp	6.71	1.87		~4[71]	−0.1[60]	−4.3[61]	1.24−1.4[c]	0.9−1.1	1.82
additive 2	7.21	1.87	1.76	2.42	0.83	−3.1	1.45	1.92	2.1
polarizable	6.72	1.83	2.01	4.12	−0.11	−4.4	1.2	1.51	2.3
additive 1[15]	7.27	1.88	1.64	2.57	0.92	−3.71	1.44		

[a] Computed in this work using the protocol described in the text. The self-energy of the halothane molecule was subtracted from the results on free energy of solvation. The electrostatic, repulsive, and dispersive components for the self-free energy were obtained from FEP/MD performed in the gas phase using Langevin dynamics with exactly the same sampling as for regular FEP/MD simulations. The self-energy for the polarizable model is estimated at −2.7 and −0.4 kcal/mol for the additive model. [b] Includes the size-dependent hydrodynamic correction of Yeh and Hummer.[59] Experimental data from refs 57 and 58. [c] The dipole moment of halothane in the gas phase was obtained from Pluhackova and Hobza on the basis of RI-MP2/cc-pVTZ level minimization[20] and from measurements reported for halothane solvation in chloroform.[55]

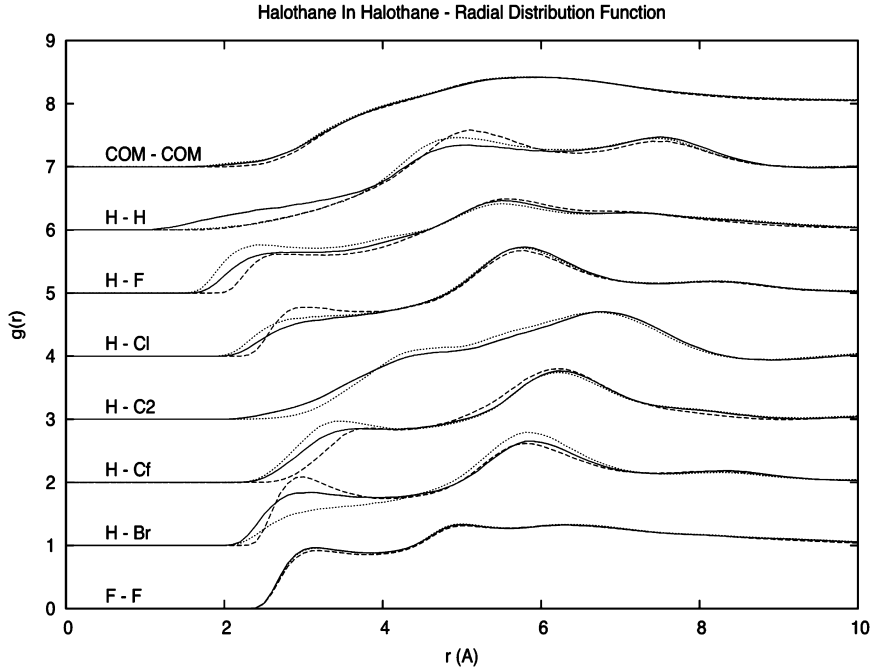

Figure 1. Radial distribution functions (RDFs) for halothane in Halothane, $g(r)$. The RDFs were done with various intermolecular atom pairs (e.g., H−Br, refers to an RDF of a hydrogen and bromine of different halothane molecules), and the COM−COM pair is the center of mass−center of mass RDF. The RDFs of different atom pairs were offset by 1 to ensure clarity. Solid black line: additive model developed in this work. Dotted line: additive model developed in ref 15. Dashed line: polarizable model developed in this work.

well with experimental results. The computed density of liquid halothane for the polarizable model differs from experiments by 0.04 g/cm^3 or ~2.1% of error (Table 2), while the currently developed and previously published additive models provide a somewhat better density description. In conclusion, all models were found to be capable of correct description for the molecular density of halothane. Three different diffusion coefficients were evaluated for the developed additive and polarizable models of halothane. In particular, we computed self-diffusion coefficients of halothane in halothane, water, and methanol. The resulting numbers are summarized in Table 2, in comparison to the available experimental data on halothane diffusion in water and methanol.[57,58] All studied models slightly overestimate the diffusion coefficients, which can be attributed in part to the finite-size effects of the relatively small boxes used in the simulations.[59]

The structure of the liquid can be characterized by a number of radial-distribution functions (RDFs). In-depth analyses of RDFs for halothane have been published previously.[15] The RDFs for all models developed in this work are apparently in agreement with each other and with previously published structural analysis. The greatest discrepancy between the additive and polarizable models is present with the involvement of the heavy halogen atoms. This can be accounted for by the presence of the auxiliary Drude particles and the temporary dipoles that they create on their host atoms. For example, the first peak in the H−Br RDF around $r = 3$ Å is much more pronounced for the polarizable model, indicating a much stronger interaction between the two atoms than for the other models (Figure 1). The dipole created around the polarizable bromine generates a more attractive electric field for the positive hydrogen to interact with; similar effects are observed for the H−Cl RDF. Moreover, the greater proximity of intermolecular H−F atoms versus H−H atoms characterized by the peak of H-F occurring much earlier than that of H−H support an antiparallel configuration of adjacent halothane molecules in its liquid phase as previously proposed.[15]

Free Energy of Halothane Solvation in Aqueous and Nonaqueous Solvents. The ability to accurately reproduce various absolute solvation free energies, ΔG_{solv} is of paramount importance for a force field intended for the study of structure and dynamics of solutes in various dielectric environments. To the best of our knowledge, the only theoretical study of the hydration free energy of halothane is that of Chambers et al.[60] Tables 2 and 3 list absolute free energies of halothane solvation in water, *n*-hexane, and methanol for all models studied in

TABLE 3: Absolute Free Energies of Halothane Solvation in Different Solvents at $T = 298.15$ K[a]

	halothane in water			halothane in methanol			halothane in *n*-hexane		
	additive 1	additive 2	Drude	additive 1	additive 2	drude	additive 1	additive 2	Drude
ΔG_{elec}	−0.60	−0.61	−0.51	−1.3	−0.7	−1.6	−2.7	−1.85	−3.4
ΔG_{disp}	−14.1	−14.3	−12.1	−13.1	−10.7	−13.9	−13.1	−12.9	−12.2
ΔG_{rep}	15.6	15.7	12.5	11.3	8.2	11.0	11.5	11.1	12.4
ΔG_{solv}	0.92	0.83	−0.11 (∼0)	−3.1	−2.7	−4.5 (−4.2)	−4.3	−4.7	−3.2 (−3.3)

[a] All free energies are reported in kcal/mol. The values in parenthesis were estimated from experimental data on the gas−liquid partitioning reported by Johannson.[61]

comparison with available experimental data[61] on the gas/liquid partitioning of halothane. These results were obtained without any further adjustments to the additive or polarizable potential models. Even with very encouraging results for solvation thermodynamics in water and neat halothane, discrepancies between theoretical and experimental absolute solvation free energies start to emerge for the solvation in organic solvents with different polarity. Experimentally, halothane displays a preferential solvation in the amphipathic solvents such as alcohols, whereas its solvation in alkanes or benzene is less favorable. The free energies of halothane solvation in methanol and hexane computed with the two additive potential models suggest preferential halothane solvation in *n*-hexane, as compared to methanol. An inclusion of the electronic polarizability into the potential function leads to a somewhat better performance in free energies. The errors in computed contributions to the free energies are on the order of ±0.7 kcal/mol, as evaluated from block-averages in WHAM analysis (every 100 ps).

A useful approach to understanding the discrepancies in the results of free energy computations with additive and polarizable models is a decomposition of the absolute solvation free energy into its principal components. It should be noted that this decomposition is path-dependent, but the resulting absolute free energy is not. Nevertheless, these components of free energies can be used as indicators for the relative importance of different contributions. There are clear differences in the electrostatic and nonelectrostatic components of the absolute solvation free energies between water and methanol solvents. The increase in the electrostatic component in the case of solvation in methanol may suggest that dipole−dipole interactions between halothane and methanol play an important role in the formation of preferential solvation in methanol. The net contribution of the nonelectrostatic term (*dispersion* + *repulsion*) is also more favorable in methanol than in water, providing an additional source for the preferential solvation of halothane. Pohorille and Wilson[62] have shown that reversible work of a cavity creation for a nonpolar molecule in water is greater than that in a less polar phase, so this result is not entirely unexpected. Therefore, an increase in favorable dispersive interactions traditionally explained within the framework of the hydrophobic effect plays the dominant role in a favorable halothane partitioning to methanol. The difference in the electrostatic component of the solvation free energy between water and methanol systems is about ∼−1 kcal/mol, whereas a similar difference between nonelectrostatic contributions is ∼−3.3 kcal/mol. This finding emphasizes an importance of the hydrophobic interactions, which is not merely a compliment to the hydrogen-bonding potency of halothane.[63−65] Comparing solvation in *n*-hexane and methanol, one may note that an ability forming hydrogen-bond-like interaction between halothane's C−H and methanol's O−H group contributes about 25% to the favorable partitioning to methanol.

TABLE 4: Solvation Thermodynamics for Different Potential Models of Halothane in Methanol[a]

	halothane in methanol		
	system 1	system 2	system 3
ΔG_{elec}	−4.7	−2.1	−2.3
ΔG_{disp}	−12.6	−15.9	−15.3
ΔG_{rep}	11.9	15.1	14.8
ΔG_{solv}	−4.9	−2.9	−2.8

[a] System 1: polarizable halothane in additive solvent MeOH. System 2: additive model developed in this paper in the polarizable solvent. System 3: model of Liu et al.[15] in the polarizable solvent.

An interesting question is about the usefulness of the explicit accounting for polarization, which is costly and slower when compared to traditional force fields. To put our model to the test, we have computed absolute free energies of halothane solvation in methanol for the following systems: polarizable halothane in additive methanol and additive halothane (both models used in our study) in polarizable methanol. This computational exercise is to test sufficiency in increasing the solvent's or solute's dipole moments implicitly including electronic polarization; results of these computations are shown in the Table 4. The results suggest that accurate accounting for the solute polarizability while implicitly accounting for solvent dynamics provides a fair description of the solvation free energy. The fixing of the halothane's dipole moment at $\mu = 1.4-1.5$ D led to underestimation the electrostatic component in computed free energies, while the net LJ contribution closely resembles simulations with polarizable force fields (∼−0.7−0.8 kcal/mol).

Halothane−Methanol Mixtures: Structure and Coordination Numbers. Analyzing the actual structure of the solvent around halothane molecules and its propensity to form hydrogen bonds to either water or methanol is now noteworthy. The different sets of halothane−solvent site pair RDF are shown on the Figure S2 in the Supporting Information. The C−H group of halothane may play an important role in the asymmetric solvent distribution around the solute molecule. The presence of the relatively polar C−H bond leads to a shift in the position of the first maxima on the RDF between C2 and the solvent's oxygen as compared to a similar function for C1 and water or methanol. The RDF between the C2 site in halothane and the polar oxygen of methanol or water displays a well-pronounced first maximum at around 3.4 Å and a shallow minimum at around 4.1−4.2 Å. This corresponds to the canonical distance between heavy atoms in direct hydrogen bonding (most probable distance for the formation of the pair). A running integration to the position of the first minima gives a coordination number around 0.9, suggesting that in diluted halothane solutions in methanol every C−H group is involved in the formation of weak hydrogen bonds to the polar oxygen of methanol.

There is a defined first minimum around 2.6−2.7 Å, which corresponds to the geometric criteria for weak hydrogen bonding with a coordination number at the position of the first maxima

TABLE 5: Positions of First Maximum (R_{max}), First Minimum (R_{min}), and Coordination Number (n) of the Two Atom−Atom Radial Distribution Functions at Different Concentrations of Halothane in Halothane−Methanol Binary Systems

	$H_{halothane}-O_{methanol}$			$H_{methanol}-O_{methanol}$			$O_{methanol}-O_{methanol}$		
	R_{max}	R_{min}	n_c	R_{max}	R_{min}	n_c	R_{max}	R_{min}	n_c
0.00			1.06[a]	1.80	2.6	1.88	2.75	3.50	1.91
0.05	2.50	3.70	∼1.01	1.85	2.65	1.90	2.85	3.55	1.93
0.10	2.60	3.80	∼0.95	1.90	2.75	1.90	2.90	3.55	1.91
0.20	2.65	3.85	0.73	1.95	2.70	1.88	2.95	3.75	1.91
0.40	2.65	3.90	0.49	1.95	2.80	1.84	2.95	3.85	1.84
0.60	2.60	3.80	0.31	1.90	2.75	1.76	2.95	3.80	1.65
0.80	2.60	3.90	0.16	1.85	2.65	1.62	2.85	3.75	1.37

[a] Extrapolation for infinite dilution. All distances are in Å.

of about 1.0 for methanol and 1.01 for water (data not shown). The result is almost model-independent and is well-reproduced with additive potential models developed in this work and published before (results not shown). The data on the characteristic RDFs and coordination number in different solutions are collected in the Table 5. The number of methanol molecules in direct contact with a hydrogen atom of halothane steadily goes down as halothane concentration increases from about 1.0 at $x \sim 0.05$ to only 0.13 at $x \sim 0.8$, indicating that even at high concentrations of halothane, methanol−methanol pairs are the prevalent arrangement for the solvent, consistent with the fact that halothane can only participate in weak hydrogen-bonding interactions.

Halothane−Methanol Mixtures: Self-Diffusion, Dielectric Properties, and Aggregation Phenomena. The importance of accounting for aggregation in halothane−methanol liquids has been emphasized many times to argue for the apparent discrepancies between spectroscopic and thermodynamic data on this binary mixture.[66−69] The self-diffusion coefficients of the molecular species forming the mixture may provide valuable insights to understand the aggregation phenomena. Dependence of the dielectric constants and self-diffusion coefficients on solute concentration is shown in Figure 2a,b, respectively. The self-diffusion coefficient of halothane is only weakly dependent on the concentration of methanol. As the concentration of methanol decreases, the solute's mobility decreases steadily by approximately 10−15%. This apparent lack of a strong coupling between dynamics of solute and solvent is noteworthy. Klein and colleagues,[56] while studying DMPC saturation with halothane, also noted the absence of coupling between diffusion coefficients of halothane and the lipid's center of mass, postulating a lack of directional interactions between halothane and lipids. Our results also suggest the strengthening of favorable hydrophobic interactions between halothane molecules and the destroyed bonding network between methanol molecules. Methanol's self-diffusion coefficients started to increase at $x_1 \sim 0.6$ until they reached a maximum value at the concentrated halothane solution. This coincides with the inflection point in the excess Gibbs free energy for halothane−methanol mixtures.[17,18] The dependence of the dielectric constant on the mixture's composition is shown in Figure 2b. It is clear that with addition of halothane to the mixture, the dielectric constant deviates from ideal behavior with a shallow minimum between $0.4 < x_1 > 0.7$. One explanation for the observed concentration dependence of diffusion and dielectric properties such as an increase in the self-diffusion coefficient of methanol and minimum in dielectric constant of mixtures is an apparent disruption of hydrogen-bonded aggregates in these mixtures at high halothane concentrations, where methanol begins to mix with halothane as a singles or pairs.

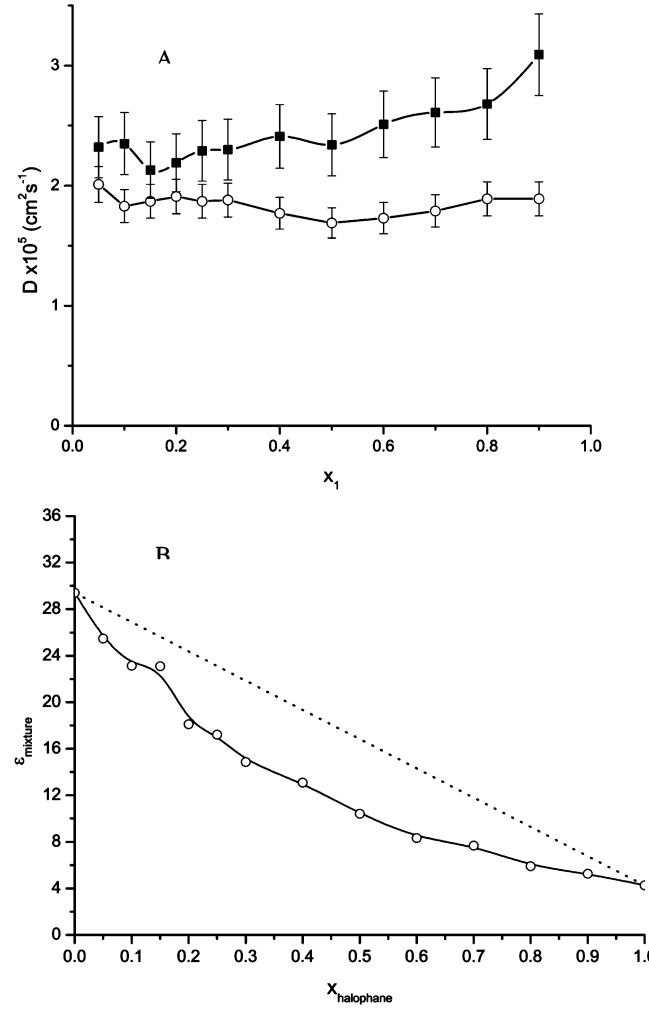

Figure 2. (a) Dependence of self-diffusion coefficients of methanol (black squares) and halothane (open circles) on the concentration of halothane. (b) Dependence of the dielectric constant for halothane−methanol mixtures on concentration (solid line with black circles) in comparison to ideal-mixing behavior (dotted line).

To test this hypothesis, a cluster size distribution analysis has been performed for different halothane−methanol admixtures. According to Figure 3, at low halothane concentrations (up to $x \sim 0.3$) most of the methanol molecules self-aggregate, whereas the percentage of the halothane−methanol clusters remains fairly small. Expectedly, there is a steady increase in the number of halothane−methanol clusters with an increase in halothane concentration, but they represent only a small fraction of particles in the system. The results on percolating methanol clusters at low concentration of halothane are reminiscent of topological analysis published previously for different

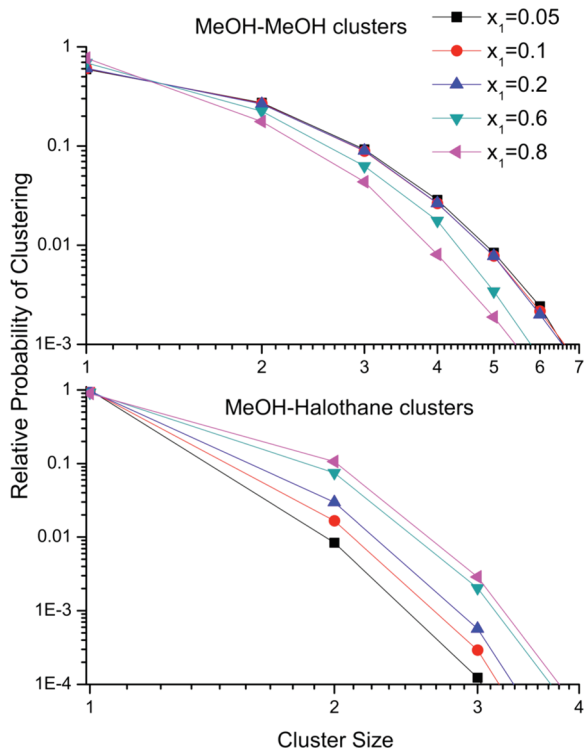

Figure 3. Relative probability for clusters with different size as function of the molar fraction of halothane. Top panel: methanol−methanol clusters. Bottom panel: mixed halothane−methanol clusters.

methanol models, suggesting that it is a robust effect.[53,68] To summarize, the hydrogen-bonding ability of halothane was found to be relatively weak and, at low concentration, alcohol molecules mainly self-aggregate. The cluster-size distributions for methanol−methanol aggregates resemble strongly pure methanol up until $X_1 > 0.2$.

4. Summary

A polarizable model for halothane was developed to reproduce the vaporization enthalpy, static dielectric constant, and self-diffusion constant of the neat liquid. It was used in combination with the polarizable SWM4-DP water and NDP−methanol models to investigate the structural and dynamical origins of the solvation in these two liquids with the capacity to form hydrogen bonds. Even though the halothane model was developed independently of the solvent model, the properties of the mixtures obtained from MD simulations are in excellent agreement with experiment. An important aspect of the polarizable model is that it reproduces the thermodynamics of solvation in water (unfavorable), methanol (favorable), and *n*-hexane (intermediate), in excellent accord with experimental data. We also evaluated the relative importance of different factors governing the solvation of halothane in amphipathic media such as methanol to mimic partitioning into the membrane interface. It was found that weak hydrogen bonding is an important factor in the asymmetric distribution of the solvent (methanol) around halothane. Meanwhile, hydrophobic interactions play an important role in the favorable halothane solvation.

Acknowledgment. This work was supported by the National Sciences and Engineering Research Council (NSERC) Discovery Grant RGPIN-315019 (S.Y.N.) and NSERC-USRA and Alberta Heritage Foundation for Medical Research Student Award (AHFMR) to J.J. S.Y.N. is an Alberta Ingenuity Fund New Faculty, Canadian Institute for Health Research New Investigator, and AHFMR Scholar.

Supporting Information Available: Tables of geometry data and frequency bands. Figures of torsion scans and radial distribution functions. This material is available free of charge via the Internet at http://pubs.acs.org.

References and Notes

(1) Bhattacharya, A. A.; Curry, S.; Franks, N. P. *J. Biol. Chem.* **2000**, *275*, 38731.
(2) Canlas, C. G.; Cui, T. X.; Li, L.; Xu, Y.; Tang, P. *J. Phys. Chem. B* **2008**, *112*, 14312.
(3) Carnini, A.; Nguyen, T. T.; Cramb, D. T. *Can. J. Chem.* **2007**, *85*, 513.
(4) Lynch, C. *Anesth. Analg.* **2008**, *107*, 864.
(5) Leonenko, Z.; Finot, E.; Cramb, D. *Biochim. Biophys. Acta, Biomembr.* **2006**, *1758*, 487.
(6) Johansson, J. S.; Scharf, D.; Davies, L. A.; Reddy, K. S.; Eckenhoff, R. G. *Biophys. J.* **2000**, *78*, 982.
(7) Vemparala, S.; Domene, C.; Kleinz, M. L. *Biophys. J.* **2008**, *94*, 4260.
(8) Tang, P.; Xu, Y. *Proc. Natl. Acad. Sci. U.S.A.* **2002**, *99*, 16035.
(9) Eckenhoff, R. G. *Mol. Interv.* **2001**, *1*, 258.
(10) Koubi, L.; Tarek, M.; Bandyopadhyay, S.; Klein, M. L.; Scharf, D. *Biophys. J.* **2001**, *81*, 3339.
(11) Tang, P.; Zubryzcki, I.; Xu, Y. *J. Comput. Chem.* **2001**, *22*, 436.
(12) Koubi, L.; Saiz, L.; Tarek, M.; Scharf, D.; Klein, M. L. *J. Phys. Chem. B* **2003**, *107*, 14500.
(13) Scharf, D.; Koubi, L.; Tarek, M.; Klein, M. *Anesthesiology* **1999**, *91*, U359.
(14) Henin, J.; Brannigan, G.; Dailey, W. P.; Eckenhoff, R.; Klein, M. *J. Phys. Chem. B* **2010**, *114*, 604.
(15) Liu, Z. W.; Xu, Y.; Saladino, A. C.; Wymore, T.; Tang, P. *J. Phys. Chem. A* **2004**, *108*, 781.
(16) Liu, L. T.; Willenbring, D.; Xu, Y.; Tang, P. *J. Phys. Chem. B* **2009**, *113*, 12581.
(17) Dohnal, V.; Tkadlecova, M. *J. Phys. Chem. B* **2002**, *106*, 12307.
(18) Tkadlecova, M.; Dohnal, V.; Costas, M. *Phys. Chem. Chem. Phys.* **1999**, *1*, 1479.
(19) Czarnik-Matusewicz, B.; Michalska, D.; Sandorfy, C.; Zeegers-Huyskens, T. *Chem. Phys.* **2006**, *322*, 331.
(20) Pluhackova, K.; Hobza, P. *ChemPhysChem* **2007**, *8*, 1352.
(21) Xu, Y.; Tang, P. *Biochim. Biophys. Acta, Biomembr.* **1997**, *1323*, 154.
(22) Davis, J. E.; Patel, S. *J. Phys. Chem. B* **2009**, *113*, 9183.
(23) Agbodjan, A. A.; Bui, H.; Khaledi, M. G. *Langmuir* **2001**, *17*, 2893.
(24) Norinder, U.; Osterberg, T. *Perspect. Drug Discov. Design* **2000**, *19*, 1.
(25) Paluch, M. *Adv. Colloid Interface Sci.* **2000**, *84*, 27.
(26) Harder, E.; MacKerell, A. D.; Roux, B. *J. Am. Chem. Soc.* **2009**, *131*, 2760.
(27) Harder, E.; MacKerell, A. D.; Roux, B. *Abstr. Pap. Am. Chem. Soc.* **2008**, *236*, 329.
(28) Harder, E.; Anisimov, V. M.; Vorobyov, I. V.; Lopes, P. E. M.; Noskov, S. Y.; MacKerell, A. D.; Roux, B. *J. Chem. Theor. Comput.* **2006**, *2*, 1587.
(29) Lamoureux, G.; Harder, E.; Vorobyov, I. V.; Roux, B.; MacKerell, A. D. *Chem. Phys. Lett.* **2006**, *418*, 245.
(30) Lamoureux, G.; MacKerell, A. D.; Roux, B. *J. Chem. Phys.* **2003**, *119*, 5185.
(31) Lamoureux, G.; Roux, B. *J. Chem. Phys.* **2003**, *119*, 3025.
(32) Lamoureux, G.; Faraldo-Gomez, J.; Krupin, S.; Noskov, S. *Chem. Phys. Lett.* **2009**, *468*, 270.
(33) Becke, A. D. *J. Chem. Phys.* **1993**, *98*, 5648.
(34) Lee, C.; Yang, W.; Parr, R. G. *Phys. Rev. B* **1988**, *37*, 785.
(35) Dunning, T. H. *J. Chem. Phys.* **1989**, *90*, 1007.
(36) Pulay, P.; Fogarasi, G.; Pang, F.; Boggs, J. E. *J. Am. Chem. Soc.* **1979**, *101*, 2550.
(37) Frisch, M. J. T., G. W.; Schlegel, H. B.; Scuseria, G. E.; Robb, M. A.; Cheeseman, J. R.; Montgomery, J. A., Jr.; Vreven, T.; Kudin, K. N.; Burant, J. C.; Millam, J. M.; Iyengar, S. S.; Tomasi, J.; Barone, V.; Mennucci, B.; Cossi, M.; Scalmani, G.; Rega, N.; Petersson, G. A.; Nakatsuji, H.; Hada, M.; Ehara, M.; Toyota, K.; Fukuda, R.; Hasegawa, J.; Ishida, M.; Nakajima, T.; Honda, Y.; Kitao, O.; Nakai, H.; Klene, M.; Li, X.; Knox, J. E.; Hratchian, H. P.; Cross, J. B.; Bakken, V.; Adamo, C.; Jaramillo, J.; Gomperts, R.; Stratmann, R. E.; Yazyev, O.; Austin, A. J.; Cammi, R.; Pomelli, C.; Ochterski, J. W.; Ayala, P. Y.; Morokuma, K.; Voth, G. A.; Salvador, P.; Dannenberg, J. J.; Zakrzewski, V. G.; Dapprich,

S.; Daniels, A. D.; Strain, M. C.; Farkas, O.; Malick, D. K.; Rabuck, A. D.; Raghavachari, K.; Foresman, J. B.; Ortiz, J. V.; Cui, Q.; Baboul, A. G.; Clifford, S.; Cioslowski, J.; Stefanov, B. B.; Liu, G.; Liashenko, A.; Piskorz, P.; Komaromi, I.; Martin, R. L.; Fox, D. J.; Keith, T.; Al-Laham, M. A.; Peng, C. Y.; Nanayakkara, A.; Challacombe, M.; Gill, P. M. W.; Johnson, B.; Chen, W.; Wong, M. W.; Gonzalez, C.; Pople, J. A. *Gaussian 03*, revision C.02; Gaussian, Inc.: Wallingford, CT, 2004.

(38) Anisimov, V. M.; Lamoureux, G.; Vorobyov, I. V.; Huang, N.; Roux, B.; MacKerell, A. D. *J. Chem. Theor. Comput.* **2005**, *1*, 153.

(39) Elola, M. D.; Ladanyi, B. M. *J. Chem. Phys.* **2005**, 122.

(40) Yin, D. X.; Mackerell, A. D. *J. Comput. Chem.* **1998**, *19*, 334.

(41) Scharf, D.; Laasonen, K. *Chem. Phys. Lett.* **1996**, *258*, 276.

(42) Anisimov, V. M.; Vorobyov, I. V.; Roux, B.; MacKerell, A. D. *J. Chem. Theor. Comput.* **2007**, *3*, 1927.

(43) Lopes, P. E. M.; Lamoureux, G.; Roux, B.; MacKerell, A. D. *J. Phys. Chem. B* **2007**, *111*, 2873.

(44) Patel, S.; Brooks, C. L. *J. Comput. Chem.* **2004**, *25*, 1.

(45) Deng, Y. Q.; Roux, B. *J. Phys. Chem. B* **2004**, *108*, 16567.

(46) Shivakumar, D.; Deng, Y. Q.; Roux, B. *J. Chem. Theor. Comput.* **2009**, *5*, 919.

(47) Shirts, M. R.; Pitera, J. W.; Swope, W. C.; Pande, V. S. *J. Chem. Phys.* **2003**, *119*, 5740.

(48) Chandler, D.; Weeks, J. D.; Andersen, H. C. *Science* **1983**, *220*, 787.

(49) Andersen, H. C.; Chandler, D.; Weeks, J. D. *J. Chem. Phys.* **1972**, *57*, 2626.

(50) Weeks, J. D.; Chandler, D.; Andersen, H. C. *J. Chem. Phys.* **1971**, *55*, 5422.

(51) Souaille, M.; Roux, B. *Comput. Phys. Commun.* **2001**, *135*, 40.

(52) Kumar, S.; Bouzida, D.; Swendsen, R. H.; Kollman, P. A.; Rosenberg, J. M. *J. Comput. Chem.* **1992**, *13*, 1011.

(53) Zhong, Y.; Warren, G. L.; Patel, S. *J. Comput. Chem.* **2008**, *29*, 1142.

(54) Baker, C. M.; MacKerell, A. D. *J. Mol. Model.* **2010**, *16*, 567.

(55) Fenclová, D.; Dohnal, V. *J. Chem. Thermodyn.* **1990**, *22*, 219.

(56) Vemparala, S.; Saiz, L.; Eckenhoff, R. G.; Klein, M. L. *Biophys. J.* **2006**, *91*, 2815.

(57) Shikii, K.; Sakurai, S.; Utsumi, H.; Seki, H.; Tashiro, M. *Anal. Sci.* **2004**, *20*, 1475.

(58) Langmaier, J.; Samec, Z. *J. Electroanal. Chem.* **1996**, *402*, 107.

(59) Yeh, I. C.; Hummer, G. *J. Phys. Chem. B* **2004**, *108*, 15873.

(60) Chambers, C. C.; Hawkins, G. D.; Cramer, C. J.; Truhlar, D. G. *J. Phys. Chem.* **1996**, *100*, 16385.

(61) Johansson, J. S.; Zou, H. *Biophys Chem* **1999**, *79*, 107.

(62) Pohorille, A.; Wilson, M. A. *J. Chem. Phys.* **1996**, *104*, 3761.

(63) Michielsen, B.; Herrebout, W. A.; van der Veken, B. J. *ChemPhysChem* **2008**, *9*, 1693.

(64) Dohnal, V.; Kratochvilova, K.; Bures, M.; Costas, M. *J. Chem. Soc., Faraday Trans.* **1996**, *92*, 1877.

(65) Brown, J. M.; Chaloner, P. A. *Can. J. Chem.* **1977**, *55*, 3380.

(66) Kiselev, M.; Noskov, S.; Puthovski, Y.; Kerdcharoen, T.; Hannongbua, S. *J. Mol. Graph Model.* **2001**, *19*, 412.

(67) Noskov, S. Y.; Kiselev, M. G.; Kolker, A. M.; Rode, B. M. *J. Mol. Liq.* **2001**, *91*, 157.

(68) Dougan, L.; Hargreaves, R.; Bates, S. P.; Finney, J. L.; Reat, V.; Soper, A. K.; Crain, J. *J. Chem. Phys.* **2005**, 122.

(69) Dougan, L.; Bates, S. P.; Hargreaves, R.; Fox, J. P.; Crain, J.; Finney, J. L.; Reat, V.; Soper, A. K. *J. Chem. Phys.* **2004**, *121*, 6456.

(70) Weinhold, F. Natural Bond Orbital Methods. In *Encyclopedia of Computational Chemistry*; Kollman, P. A., Ed.; John Wiley & Sons: Chichester, U.K., 1998; Vol. 3; pp 1792

(71) Yoshida, T.; Kamaya, H.; Ueda, I. *J. Colloid Interface Sci.* **1983**, *116*, 39.

JP908339J